

Chapter 4

High Porosity Metallic Glass Foam: A Powder Metallurgy Route

Abstract

A powder metallurgy route to the fabrication of metallic glass foam is introduced. The method involves consolidating metallic glass powder blended with blowing agent particulates to produce expandable precursors, capable of yielding foams with porosities as high as 86%. The foams are found to inherit the strength of the parent metallic glass, and to be able to deform heavily toward full densification absorbing high amounts of energy (>30 MJ/m³).

The content of this chapter was previously published in Applied Physics Letters 2007;91(16).

Introduction

The ability of amorphous metals to soften and flow upon relaxation at the glass transition gives rise to a viscoplastic flow behavior that enables unique forming capabilities, similar to those of plastics and conventional glasses [53, 54, 55]. The development of highly porous metallic glass foam via viscoplas-

tic expansion of impregnated pores has recently emerged as an attractive thermoplastic forming process [28, 39, 56, 57]. In this chapter we demonstrate that by utilizing a powder metallurgy route, an efficient foaming process is made possible by which highly porous metallic glass foam can be fabricated. The advantages of using powder metallurgy to fabricate near-net-shape metallic glass components are well documented [38, 58]. By taking advantage of the viscoplastic flow characteristics of the supercooled liquid state, highly consolidated metallic glass components have been produced having dimensions that exceed the critical casting thickness of the monolithic glass while exhibiting the thermodynamic and mechanical properties of the glass. Moreover, composite [59] or porous [43] (<40% porosity) metallic glasses have been developed by mixing metallic glass powder with fugitive acid-soluble particulates. Here we show that by mixing metallic glass powder with blowing agent particulates, expandable precursors can be fabricated capable of yielding metallic glass foams with porosities as high as 86%, able to effectively inherit the strength of the glass and to deform heavily absorbing high amounts of energy.

Methods

The method introduced here involves consolidating the powder mixture at a temperature within the supercooled liquid region of the alloy but below the decomposition point of the blowing agent to produce a foam precursor. The precursor can be subsequently expanded into foam at a temperature within the supercooled liquid region and above the decomposition point of the agent. An ideal blowing agent for the present method should therefore chemically decompose to release gas at a temperature within the supercooled liquid region of the alloy, preferably closer to the glass transition temperature, T_g .

To ensure that the precursor and the foam remain amorphous, the durations for the consolidation and expansion processes should not exceed the time for the supercooled liquid to crystallize at the respective process temperatures.

In the present study we utilize a $\text{Pd}_{43}\text{Ni}_{10}\text{Cu}_{27}\text{P}_{20}$ glass. The glass transition and crystallization temperatures of this alloy are approximately 300°C and 400°C , respectively. The alloy was prepared by first prealloying Pd (99.9% purity), Ni (99.9% purity), and Cu (99.99% purity) by induction melting, and then alloying P (99.9999% purity) by step-wise furnace heating. The alloy ingot was fluxed with B_2O_3 at 720°C , and was subsequently water quenched to the amorphous state. The glassy ingot was crushed into a fine powder and was sieved into 0.425 mm mesh. The thermal analysis scan revealing the amorphous nature of the powder is presented in figure 4.1. As a blowing agent, magnesium carbonate, n-hydrate ($\text{MgCO}_3 \cdot n\text{H}_2\text{O}$) powder from J. T. Baker was employed. Thermogravimetric analysis of this powder revealed a slight mass loss accompanied by a weak endothermic reaction at $\sim 180^\circ\text{C}$, which can be associated with the release of H_2O vapor, followed by a severe mass loss accompanied by a strong endothermic reaction at $\sim 335^\circ\text{C}$, which can be associated with the decomposition of MgCO_3 releasing CO_2 . The massive release of CO_2 at a temperature slightly above T_g suggests that by properly consolidating the powder mixture at a temperature near T_g , an enormous amount of propellant gas can be available for viscoplastic foaming within the supercooled liquid region. The slight release of H_2O vapor at 180°C is found to have a negligible effect on the consolidation process.

A uniform powder mixture with minimal segregation consisting of 95 vol% $\text{Pd}_{43}\text{Ni}_{10}\text{Cu}_{27}\text{P}_{20}$ and 5 vol% MgCO_3 was prepared. Hot isostatic pressing (HIP) was performed to consolidate the mixture (American Isostatic Presses, AIP6-30H). A stainless steel canister (19.05 mm in diameter and 65 mm in length) containing the powder mixture was first evacuated and then e-beam

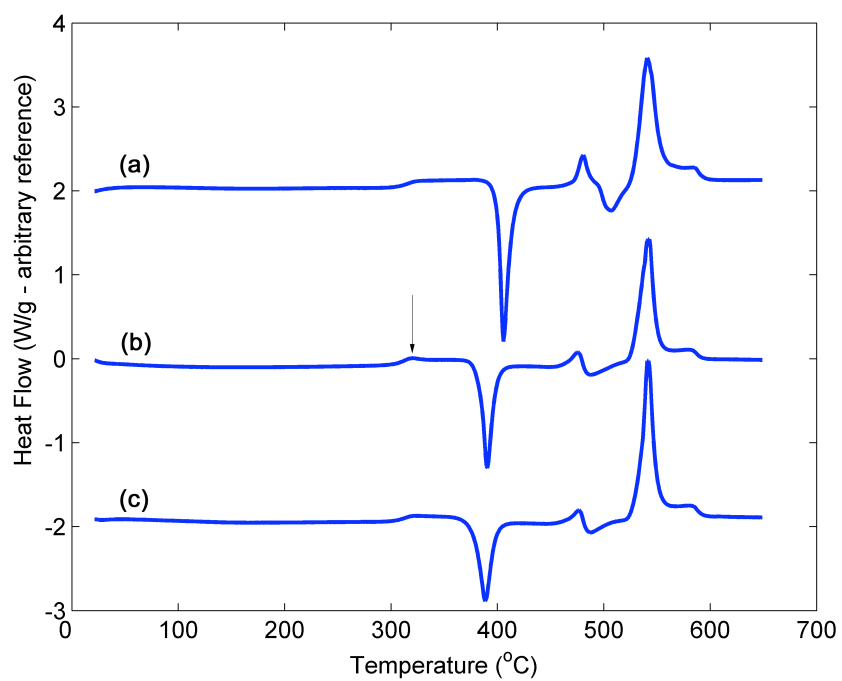


Figure 4.1: Differential calorimetry scans of the metallic glass powder (a), the precursor (b), and the foam (c). Arrow in (b) indicates a minor bump associated with the endothermic decomposition reaction of the agent.

welded. The HIP procedure consisted of applying a pressure of 207 MPa followed by a gradual temperature rise to $290 \pm 10^\circ\text{C}$. The mixture was held at the process temperature under the applied pressure for 2 hours. The density of the consolidated precursor (measured by the Archimedes method) was found to be the same as the monolithic solid to within measurement error ($9.34 \pm 0.01 \text{ g/cm}^3$). The thermal analysis scan revealing the amorphous nature of the precursor is presented in figure 4.1. The glass transition temperature of the consolidated precursor appears unchanged in reference to the glassy powder. However the crystallization temperature appears somewhat lower, possibly due to the presence of decomposed MgO acting as heterogeneous nucleant. It is interesting to note that a minor bump is observed slightly above T_g , which is consistent with the endothermic decomposition reaction of the agent.

Expansion of the consolidated precursor into foam was performed by inductively heating the precursor to a temperature within the supercooled liquid region under vacuum, holding for a period shorter than the time required for crystallization at that temperature, and subsequently quenching. Porosity was controlled by the temperature and duration of foaming. Various segments of the precursor were expanded at temperatures ranging between 340°C and 370°C for durations ranging between 10 and 100 s, accomplishing porosities that range between 4% and 86% (measured by the Archimedes method). An 82% porosity foam expanded at 350°C for 60 s is shown in figure 4.2. A precursor segment of equivalent mass is also presented alongside the foam in order to demonstrate the fivefold increase in volume produced by foaming. The fully glassy nature of the foam is verified by x-ray diffraction, shown in the inset of figure 4.2. The thermal analysis scan revealing the thermodynamic characteristics of the foam is presented in figure 4.1. Like the precursor, the foam exhibits a glass transition temperature consistent

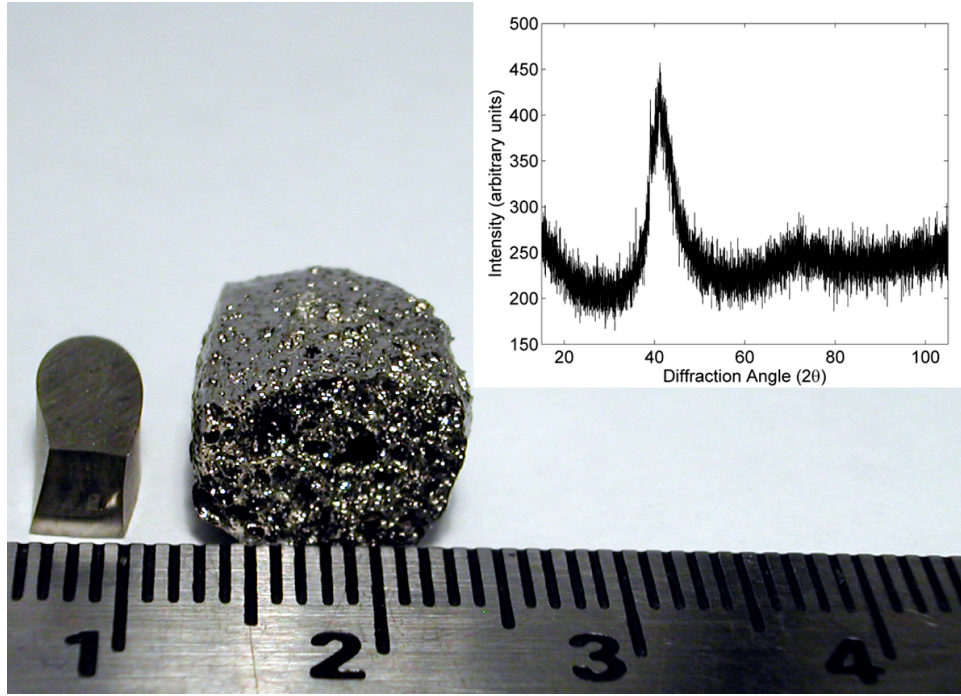


Figure 4.2: Image of an 82% porosity foam produced via the introduced powder metallurgy route, alongside a precursor segment of equivalent mass. Inset: X-ray diffractogram verifying the amorphous nature of the foam.

with the reference powder but a crystallization temperature that is slightly lower.

Results and Discussion

The microstructure of the consolidated precursor and the cellular structure of the 82% porosity foam were examined using scanning electron microscopy. A magnified view of a radial cross section of the precursor is shown in the micrograph of figure 4.3(a). The grooves between metallic-glass particulates are thin, and filled with blowing agent powder. The micrograph of figure 4.3(b) shows a highly magnified view of an interparticulate groove filled with blow-

ing agent powder. The chemical composition of the agent particulate agglomerates was verified by energy dispersive x-ray analysis. A magnified view of a radial cross section of the foam is shown in the micrograph of figure 4.3(c). A distribution of pore sizes is observed with a mean pore size on the order of 300–400 μm . Small amounts of blowing agent agglomerates can be detected within smaller pores, indicating that a small fraction of the blowing agent failed to fully decompose during expansion. Closer inspection in the vicinity of the solid region of the foam, presented in the micrograph of figure 4.3(d), reveals that the bonding between particles has improved considerably following foaming, an effect that can be attributed to the viscoplastic shear flow realized upon expansion. Consolidated struts with good particulate bonding can be expected to exhibit a strength close to the strength of the metallic glass, giving rise to a global foam strength consistent with the strength of the parent solid.

Compressive testing of foams with porosities of 4%, 40%, and 86% was performed. Square specimens with adequate homogeneity and sufficient number of cells per side having aspect ratios ranging between 1.2 and 1.5 were prepared. Strain rates of $1 \times 10^{-4} \text{ s}^{-1}$ were applied. Strains were measured using a linear variable differential transformer. The compressive stress-strain responses are shown in figure 4.4. The 4% porosity foam is shown to yield at a relatively high stress (650 MPa), however is able to undergo only minimal plastic deformation before failing catastrophically by an incipient collapse event. The 40% porosity foam fails at a lower stress (225 MPa), however since the principal collapse is non-catastrophic, the foam is able to undergo considerable plastic deformation at a plateau stress that is approximately 50% of the yield stress. It is interesting to note that the failure characteristics of the present 40% porosity foam are similar to the 40% porosity foam reported in ref. [43], which likewise fails by an incipient non-catastrophic collapse event

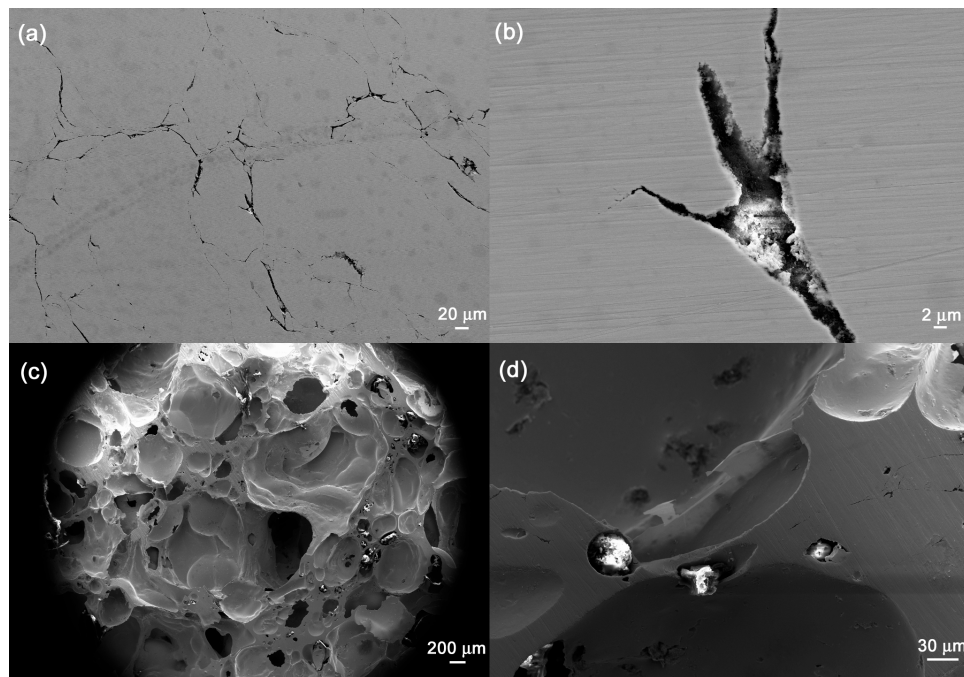


Figure 4.3: Scanning electron micrographs showing the microstructure of the precursor (a) and (b), and the cellular structure of an 82% foam (c) and (d).

characterized by a stress drop in excess of 30%. In contrast, the 86% porosity foam produced here yields at a considerably lower stress (25 MPa), however is capable of maintaining a plateau stress that is on average comparable to the failure stress. Consequently, as shown in figure 4.5, the 86% porosity foam is able to undergo plastic deformation to 80% strain. The densification strain of a foam ε_D , which together with the plateau stress dictate the foam energy absorption capability, is determined solely from the relative density ρ^*/ρ_s (in the limit of low ρ^*/ρ_s) according to $\varepsilon_D = 1 - 1.4(\rho^*/\rho_s)$ [24].

Thus, the densification strain for an 86% porosity foam can be estimated to be $\sim 80\%$, revealing that the present 86% porosity foam is capable of being deformed to ε_D . Due to a relatively high and, on average, constant plateau stress, the foam is thus able to absorb a considerable amount of mechanical energy prior to being fully densified. The specific energy absorbed by this foam can be estimated from the area under the stress-strain curve to be 31 MJ/m³. This value is nearly twice the value reported for another 86% porosity metallic glass foam [34]. The higher energy absorption capability of the present foam is attributed to its ability to maintain a relatively high plateau stress, which on average is higher than that of ref. [34] by nearly a factor of 2 (even though the parent metallic glass of ref. [34] is 10% stronger).

As discussed above, because of a well-consolidated strut microstructure, foam strengths that are consistent with the strength of the parent solid can be expected. Hence, we will attempt to correlate the foam failure stresses to the plastic yield strength of the glass. In the inset of figure 4.4, the foam failure stresses σ_y normalized by the solid plastic yield strength σ_{ys} (known to be 1630 MPa for Pd₄₃Ni₁₀Cu₂₇P₂₀ [29]) are plotted against ρ/ρ_s . The power law correlation for plastically yielding foams, given by $\sigma_y/\sigma_{ys} = 0.3(\rho/\rho_s)^{3/2}$ [24], is also plotted. The data for the 40% and 86% porosity foams appear to conform remarkably well to the established correlation, indicating that the

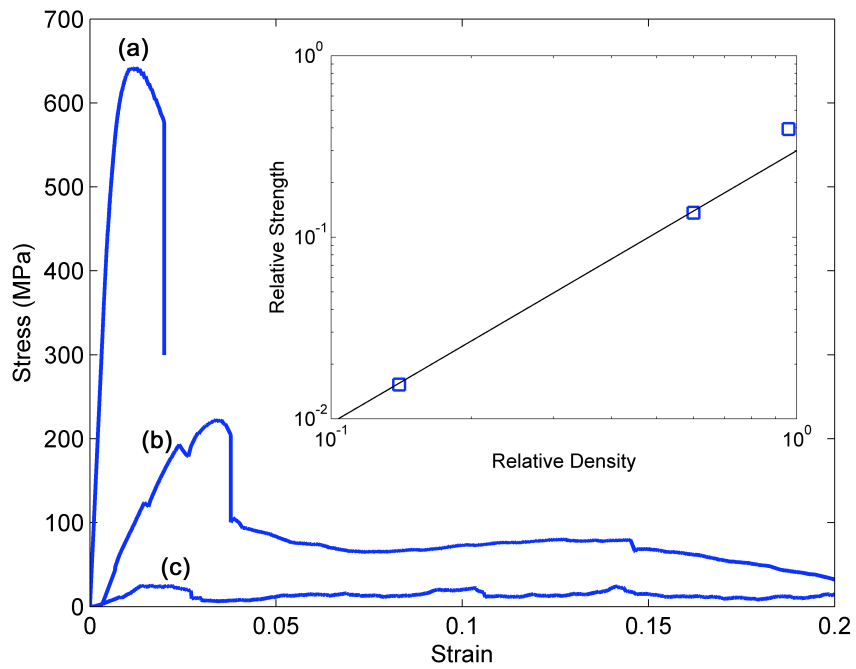


Figure 4.4: Compressive stress-strain diagrams of 4% (a), 40% (b), and 86% (c) porosity foams. Inset: Foam relative strengths plotted against relative densities. The solid line is a plot of the power law correlation established for plastically yielding foams [24].

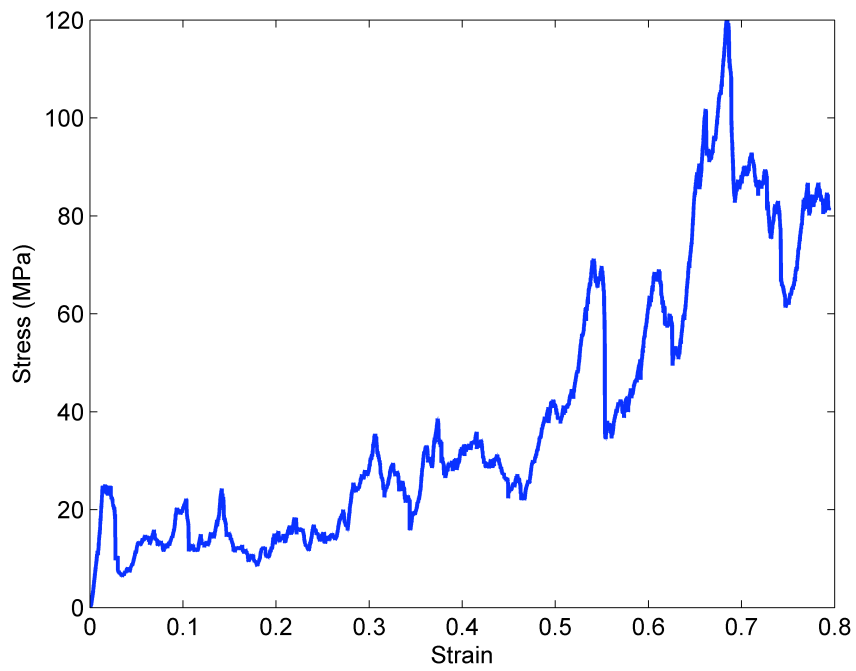


Figure 4.5: Compressive stress-strain diagram of an 86% porosity foam deformed toward full densification.

strengths of these foams scale consistently with the plastic yield strength of the parent glass. The slight deviation of the 4% porosity foam is attributed to the expected breakdown of the correlation at high relative densities [24]. It is also interesting to note that the Youngs moduli of these foams, which are estimated from the initial linear loading responses to be 95.7 GPa, 10.3 GPa, and 1.41 GPa for porosities 4%, 40%, and 86% respectively, scale reasonably with the solid Youngs modulus (reported to be 102 GPa [29]).

Conclusions

In summary, a powder metallurgy route to the fabrication of metallic glass foam was introduced. It was demonstrated that by consolidating metallic glass powder blended with blowing agent particulates, expandable metallic glass precursors could be produced which were capable of plastically yielding foams with porosities as high as 86%. The foams effectively inherit the high strength of the parent metallic glass, and are able to deform heavily towards full densification absorbing high amounts of energy.

Authors would like to acknowledge valuable discussions with J. Schroers and to express their gratitude to G. Garret and M. M. Palos for the valuable assistance.